Supporting Information for

Understanding the catalytic performances of metal-doped Ta_2O_5 catalysts for acidic oxygen evolution reaction with computations

Congcong Han,[1,2] Tao Wang[2,3,4*]

[1]Department of Chemistry, Zhejiang University, Hangzhou 310058, Zhejiang Province, China.

[2]Center of Artificial Photosynthesis for Solar Fuels and Department of Chemistry, School of Science and Research Center for Industries of the Future, Westlake University, 600 Dunyu Road, Hangzhou 310030, Zhejiang Province, China.

[3]Institute of Natural Sciences, Westlake Institute for Advanced Study, 18 Shilongshan Road, Hangzhou 310024, Zhejiang Province, China.

[4]Division of Solar Energy Conversion and Catalysis at Westlake University, Zhejiang Baima Lake Laboratory Co., Ltd, Hangzhou 310000, Zhejiang, China.

Email: twang@westlake.edu.cn

CONTENTS

Supporting Note 1: Reaction mechanism of OER

In the water-splitting reaction, hydrogen evolution reaction(HER) and oxygen evolution reaction(OER) occur at the cathode and anode, respectively. The catalytic activities of catalysts for OER are evaluated through the determination of the theoretical overpotential η_{OER} and the potential-determining step (PDS). The classic adsorbate evolution mechanism(AEM) used in this work involved $^*O$, $^*OH$, and $^*OOH$ as key reaction intermediates.[1, 2] Specifically, the four proton and electron transfer steps under acidic conditions for the $4e^-$ OER mechanism are:

$$2H_2O \rightarrow O_2(g) + 2H_2(g) \quad (1)$$

$$H_2O + * \rightarrow {}^*OH + H^+ + e^- \quad (1a)$$

$$^*OH \rightarrow {}^*O + H^+ + e^- \quad (1b)$$

$$^*O + H_2O \rightarrow {}^*OOH + H^+ + e^- \quad (1c)$$

$$^*OOH \rightarrow * + O_2 + H^+ + e^- \quad (1d)$$

Where *, $^*OH$, $^*O$, $^*OOH$ represents the clean surface and hydroxyl, oxygen, and hydroperoxide intermediates on the surface, respectively. [3]

The Gibbs free energy change for steps 1a-1d can be expressed as 2a-2d.

$$\Delta G_1 = \Delta G_{*OH} - \Delta G_{*H_2O(l)} + \Delta G_{H^+}(pH) - eU \quad (2a)$$

$$\Delta G_2 = \Delta G_{*O} - \Delta G_{*OH} + \Delta G_{H^+}(pH) - eU \quad (2b)$$

$$\Delta G_3 = \Delta G_{*OOH} - \Delta G_{*O} + \Delta G_{H^+}(pH) - eU \quad (2c)$$

$$\Delta G_4 = 4.92[eV] - \Delta G_{*OOH} + \Delta G_{H^+}(pH) - eU \quad (2d)$$

The free energy change of the protons relative to a specified electrode at non-zero pH is described by the Nernst equation as $\Delta G_{H^+}(pH) = -k_B T \ln[H^+] = k_B T \ln(10) \times pH$. The computational hydrogen electrode (CHE) is used to express the chemical potential of the proton-electron pair $H^+ + e^-$, which correlates it with the chemical potential of the gas-phase H_2 molecule based on the equilibrium $\mu[H^+] + \mu[e^-] = 1/2\mu[H_2(g)]$ at 0 V_{SHE} (Where SHE is the standard hydrogen electrode).[4] To avoid the use of O_2 electronic energy, which is difficult to determine accurately within standard GGA-DFT, the experimental free energy of $2H_2O(l) \rightarrow O_2(g) + 2H_2(g)$, $\Delta G = 4.92$ eV is used. The Gibbs free energies of reaction 2a-2b depend on the free energies of the reaction

intermediates (ΔG_{*OH}, ΔG_{*O}, ΔG_{*OOH}) calculated relative to H_2O(g) and H_2(g) at U = 0 V and standard conditions (T = 298.15 K and p = 1 bar, and pH = 0). The binding energies of $^*O$, $^*OH$, $^*OOH$ on the different surface terminations, including M-termination ($Ta_{16}O_{40}$ and M-$Ta_{15}O_{40}$), O-termination ($Ta_{16}O_{42}$ and M-$Ta_{15}O_{42}$), and the surface determined by surface Pourbaix diagrams, were systematically calculated with DFT. Multiple sites for $^*O$, $^*OH$, $^*OOH$ on various surfaces were considered, and the most stable configurations were used to determine Gibbs free energies. The Gibbs free energy differences of these intermediates include zero point energy (ZPE) and entropic corrections according to $\Delta G_i = \Delta E_i + \Delta ZPE - T\Delta S_i$ and energy differences ΔE_i calculated relative to H_2O and H_2 (at U = 0 and pH = 0) as:

$$\Delta E_{*OH} = E(^*OH) - E(*) - [E(H_2O) - \tfrac{1}{2}E(H_2)] \quad (3a)$$

$$\Delta E_{*O} = E(^*O) - E(*) - [E(H_2O) - E(H_2)] \quad (3b)$$

$$\Delta E_{*OOH} = E(^*OOH) - E(*) - [2E(H_2O) - \tfrac{3}{2}E(H_2)] \quad (3c)$$

The theoretical overpotential is then defined as:

$$\eta = \max[\Delta G_1, \Delta G_2, \Delta G_3, \Delta G_4]/e - 1.23 \quad (4)$$

Note that the theoretical overpotential given by eq. 4 is only a thermodynamic quantity, but it has been found to scale well with measured overpotentials, which depend on the concentration of active sites and the current density.

Supporting Note 2: Stability of the M-doped surface

The formation energy (E_f) is defined in eq.5 as $E_f = E_{M\text{-doped}} + E_{Ta} - E_{slab} - E_M$, where a more negative value of E_f indicates a relatively higher synthetic feasibility. Here, $E_{M\text{-doped}}$ and E_{slab} represent the electronic energy of the doped and undoped systems, respectively. E_M is the energy of a dopant metal atom in its bulk. Regarding the energy of the substituted Ta atom (E_{Ta}), we used its energy in bulk Ta_2O_5 ($E_{Ta} = 1/2 \times (E_{Ta2O5} - 5E_O)$, where E_{Ta2O5} is the electronic energy of stoichiometric bulk Ta_2O_5, and E_O is referred to H_2O/H_2 ($E_O = E_{H2O} - E_{H2}$).

The cohesive energy (E_{coh}) is defined in eq. 6 as $E_{coh} = (n_M E_M + n_{Ta} E_{Ta} + n_O E_O - E_{M\text{-doped}}) / (n_M + n_{Ta} + n_O)$, where n_M, n_{Ta}, and n_O denote the numbers of dopant, Ta, and

O in the systems.

Supporting Note 3: Surface Pourbaix diagrams

We construct the surface Pourbaix diagram to identify the electrochemically most stable structures for undoped and M-doped Ta_2O_5(100) at a range of potentials and pH values. It is noted that Ta_2O_5 bulk is stable in acid and alkaline environments. The surface Pourbaix diagrams are constructed by eq. 7a-7g, where $E(n^*O + y^*OH)$ is the total energy of a surface with n *O and y *OH, E_{slab} is the total energy of the bare surface, $E(H_2)$ is the total energy for gas phase hydrogen molecule, and $E(H_2O)$ is the total energy of gas phase water molecule.[5]

$$(n + y)H_2O + (n + y)^* \rightarrow n^*O + y^*OH + (n + \frac{y}{2})H_2 \quad (7a)$$

$$\Delta E_{total} = E(n^*O + y^*OH) + (n + \frac{y}{2})E(H_2) - [(n + y)E(H_2O) + E_{slab}] \quad (7b)$$

$$\Delta E_{ZPE} = E_{ZPE}(n^*O + y^*OH) + (n + \frac{y}{2})E_{ZPE}(H_2) - (n + y)E_{ZPE}(H_2O) \quad (7c)$$

$$T\Delta S = TS\ (n^*O + y^*OH) + (n + \frac{y}{2})TS(H_2) - (n + y)TS(H_2O) \quad (7d)$$

$$\mu(H^+) + \mu(e^-) = G(H^+) + G(e^-) = \frac{1}{2}G(H_2) \quad (7e)$$

$$\Delta G(0,0) = \Delta G = \Delta E_{total} + \Delta E_{ZPE} - T\Delta S \quad (7f)$$

$$\Delta G(pH,U) = \Delta G(0,0) + \Delta G_{H^+}(pH) - eU \quad (7g)$$

Table S1. The total energies (eV) of possible doping positions of M-$Ta_{15}O_{40}$ and M-$Ta_{15}O_{42}$

	M-$Ta_{15}O_{40}$		M-$Ta_{15}O_{42}$	
Doping position	1	2	1	2
Ti	-507.9009	**-507.9494**	-516.3548	**-516.6749**
V	-506.7620	**-506.9128**	**-518.6498**	-517.5882
Cr	-505.8880	**-506.0495**	-516.6138	**-516.9331**
Mn	-505.0278	**-505.3196**	-514.1780	**-514.9431**
Fe	-503.1648	**-503.2061**	-511.0734	**-511.9281**
Co	-500.4849	**-500.6487**	-508.4005	**-509.2293**
Ni	-497.8923	**-498.0494**	-505.4779	**-505.8334**
Zr	**-510.4981**	-510.4699	**-519.1330**	-518.7411
Nb	**-508.6534**	-508.5749	-519.8107	**-519.8669**
Mo	-506.8909	**-507.0098**	-519.4780	**-520.1699**
Ru	-502.3722	**-502.8531**	-513.0474	**-514.1804**
Sn	-500.1086	**-500.3193**	**-508.5416**	-508.4985
Sb	-500.0948	**-500.238**4	-509.0633	**-509.3030**
Ir	-500.8445	**-501.4327**	-511.1992	**-512.6152**
$Ta_{16}O_{40}$	-511.1941		$Ta_{16}O_{42}$	-522.4311

Note: 1 represents the left doping site, 2 means the right doping site. **Bold numbers** represent doping site with the lowest energy.

Table S2. Formation energy (E_f), cohesive energy (E_{coh}) of M-$Ta_{15}O_{40}$ and M-$Ta_{15}O_{42}$

M	E_f(eV)	E_{coh} (eV/atom)	M	E_f(eV)	E_{coh} (eV/atom)
Ti	-4.032	0.757	Ti	-1.520	0.633
V	-1.908	0.719	V	-2.408	0.649
Cr	-0.544	0.695	Cr	-0.191	0.611
Mn	-0.317	0.691	Mn	1.297	0.585
Fe	1.106	0.665	Fe	3.621	0.545
Co	2.425	0.642	Co	5.082	0.520
Ni	3.458	0.623	Ni	6.911	0.488
Zr	-5.840	0.789	Zr	-3.238	0.663
Nb	-2.510	0.730	Nb	-2.487	0.650
Mo	-0.089	0.687	Mo	-2.012	0.642
Ru	2.315	0.644	Ru	2.225	0.569
Sn	-0.253	0.690	Sn	2.762	0.560
Sb	0.104	0.683	Sb	2.276	0.568
Ir	3.333	0.626	Ir	3.387	0.549
$Ta_{16}O_{40}$	-	0.744	$Ta_{16}O_{42}$	-	0.664

Table S3. ΔG (eV) of each step during OER and theoretical overpotential on the M-$Ta_{15}O_{40}$ at standard conditions.

M	ΔG_{*OH}	ΔG_{*O}	ΔG_{*OOH}	$\Delta G_{*O} - \Delta G_{*OH}$	η(V)	PDS
Ti	-0.022	1.920	3.517	1.942	0.712	$^*OH \rightarrow {}^*O$
V	-0.669	0.186	2.766	0.855	1.350	$^*O \rightarrow {}^*OOH$
Cr	-0.238	0.710	3.250	0.946	1.311	$^*O \rightarrow {}^*OOH$
Mn	0.475	1.956	3.950	1.482	0.766	$^*O \rightarrow {}^*OOH$
Fe	0.236	2.154	3.968	1.918	0.688	$^*OH \rightarrow {}^*O$
Co	0.171	2.122	3.978	1.951	0.721	$^*OH \rightarrow {}^*O$
Ni	0.271	2.233	3.728	1.963	0.733	$^*OH \rightarrow {}^*O$
Zr	-0.196	1.815	3.359	2.011	0.781	$^*OH \rightarrow {}^*O$
Nb	-1.108	-0.448	2.414	0.660	1.632	$^*O \rightarrow {}^*OOH$
Mo	-0.870	-0.586	2.611	0.285	1.967	$^*O \rightarrow {}^*OOH$
Ru	0.349	1.171	3.408	0.822	1.007	$^*O \rightarrow {}^*OOH$
Sn	0.129	2.325	3.584	2.196	0.966	$^*OH \rightarrow {}^*O$
Sb	0.710	1.513	4.229	0.803	1.487	$^*O \rightarrow {}^*OOH$
Ir	0.214	1.214	3.201	0.999	0.758	$^*O \rightarrow {}^*OOH$
$Ta_{16}O_{40}$	-1.236	-0.599	2.287	0.637	1.656	$^*O \rightarrow {}^*OOH$
Pt(111)	0.999	1.393	3.852	0.394	1.229	$^*O \rightarrow {}^*OOH$

Table S4. ΔG (eV) of each step during OER and theoretical overpotential on the M-$Ta_{15}O_{42}$ at standard conditions.

M	ΔG_{*OH}	ΔG_{*O}	ΔG_{*OOH}	$\Delta G_{*O} - \Delta G_{*OH}$	η(V)	PDS
Ti	2.426	4.485	5.286	2.059	1.196	$* \rightarrow {}^*OH$
V	3.090	5.493	6.121	2.402	1.860	$* \rightarrow {}^*OH$
Cr	2.081	4.183	4.806	2.101	0.871	$^*OH \rightarrow {}^*O$
Mn	2.297	4.449	4.783	2.152	1.067	$* \rightarrow {}^*OH$
Fe	2.060	4.163	4.755	2.103	0.873	$^*OH \rightarrow {}^*O$
Co	2.081	4.163	4.806	2.082	0.852	$^*OH \rightarrow {}^*O$
Ni	2.308	4.469	4.831	2.161	1.078	$* \rightarrow {}^*OH$
Zr	2.248	4.353	4.694	2.104	1.018	$* \rightarrow {}^*OH$
Nb	2.137	3.988	4.790	1.852	0.907	$* \rightarrow {}^*OH$
Mo	1.974	4.113	4.786	2.138	0.908	$^*OH \rightarrow {}^*O$
Ru	1.955	4.109	4.805	2.154	0.924	$^*OH \rightarrow {}^*O$
Sn	2.088	4.249	4.826	2.161	0.931	$^*OH \rightarrow {}^*O$
Sb	1.913	3.868	4.744	1.954	0.724	$^*OH \rightarrow {}^*O$
Ir	1.518	3.830	4.692	2.312	1.082	$^*OH \rightarrow {}^*O$
$Ta_{16}O_{42}$	1.995	4.006	4.784	2.012	0.782	$^*OH \rightarrow {}^*O$

Table S5. Adsorption energies (eV) of the various intermediates considered on the M-doped surfaces (only the most stable configurations were summarized).

Metal	Clean surface	1/4 ML *O	1/4ML *OH	1/2 ML *OH	1/4 ML *O + 1/4 ML *OH
Ti	0	1.956	0.113	1.273	2.908
V	0	0.223	-0.267	-0.607	1.750
Cr	0	0.746	-0.187	0.089	1.723
Mn	0	1.993	0.566	1.351	3.433
Fe	0	2.122	0.356	0.631	3.896
Co	0	2.211	0.300	1.433	4.037
Ni	0	2.270	0.305	1.691	3.909
Zr	0	1.871	-0.157	1.159	3.432
Nb	0	-0.566	-1.068	-1.285	0.969
Mo	0	-0.973	-0.832	-1.178	-0.800
Ru	0	0.910	0.240	0.580	1.886
Sn	0	2.196	0.191	1.252	3.959
Sb	0	1.549	0.750	0.503	3.022
Ta_2O_5	0	-0.563	-1.165	-1.304	0.976

Table S6: ΔG (eV) of intermediate species on the most stable surface state of M-doped systems under working conditions as determined by surface Pourbaix diagrams.

Metal	ΔG_{*OH}	ΔG_{*O}	ΔG_{*OOH}	$\Delta G_{*O} - \Delta G_{*OH}$	η(V)	PDS
Ti	1.560	3.745	4.595	2.185	0.955	*OH → *O
V	0.078	2.476	3.654	2.397	1.167	*OH → *O
Cr	0.704	3.006	4.266	2.302	1.072	*OH → *O
Mn	1.171	3.271	4.282	2.099	0.869	*OH → *O
Fe	1.230	3.555	4.092	2.324	1.094	*OH → *O
Co	1.141	3.597	4.525	2.454	1.224	*OH → *O
Ni	1.298	3.480	4.130	2.182	0.951	*OH → *O
Zr	1.515	3.579	4.310	2.063	0.833	*OH → *O
Nb	0.332	2.173	3.389	1.840	0.610	*OH → *O
Mo	0.133	2.196	3.553	2.063	0.833	*OH → *O
Ru	0.940	2.135	3.980	1.195	0.614	*O → *OOH
Sn	1.461	3.728	4.528	2.266	1.036	*OH → *O
Sb	-0.075	2.778	3.362	2.853	1.623	*OH → *O
Ir	0.760	2.078	3.634	1.318	0.325	*O → *OOH
Ta_2O_5	-0.049	1.910	3.290	1.959	0.729	*OH → *O

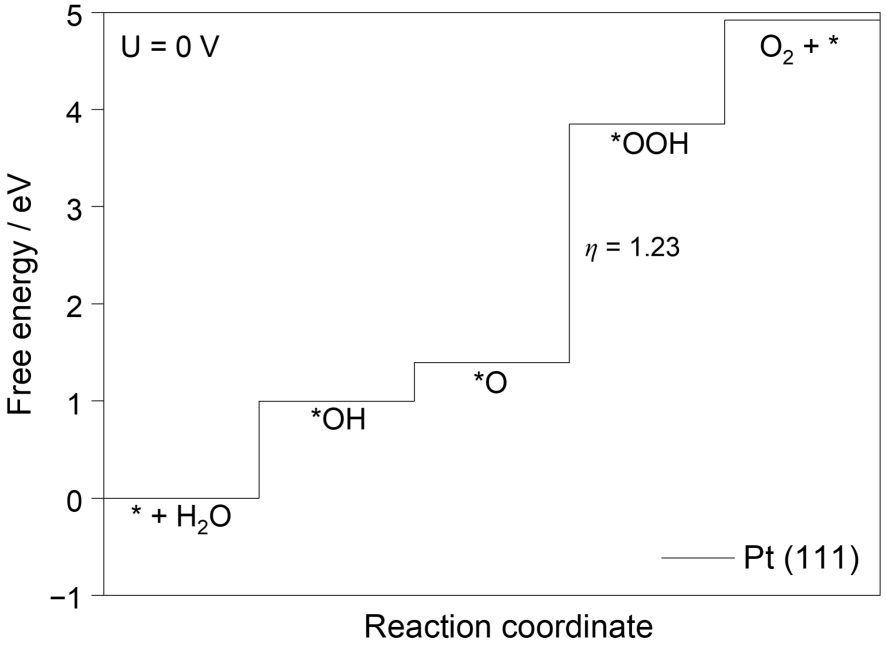

Figure S1. The free energy diagram of OER on the Pt(111) surface

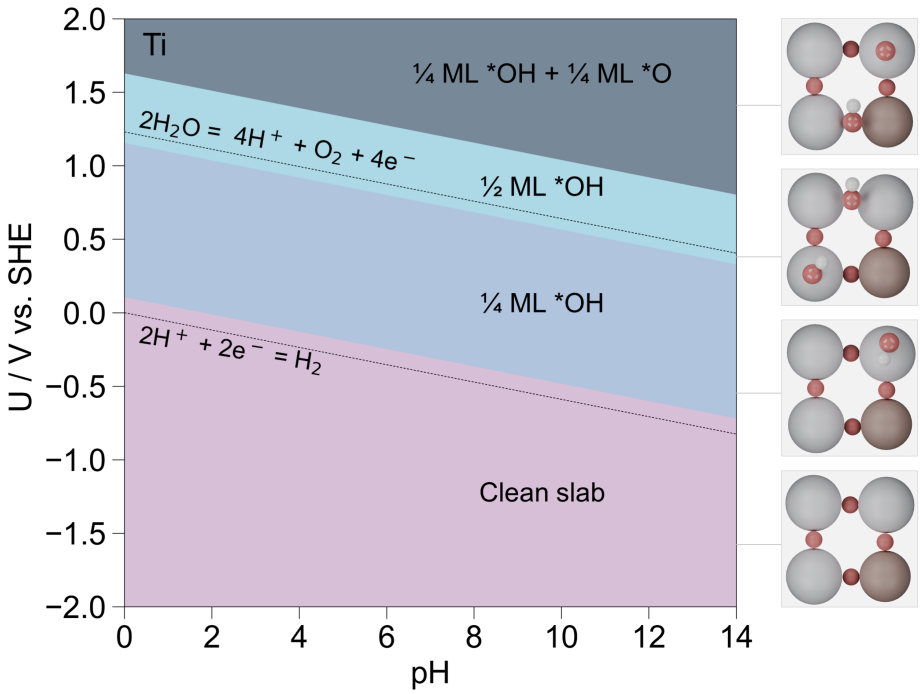

Figure S2. Surface Pourbaix diagram of Ti-doped Ta_2O_5(100)

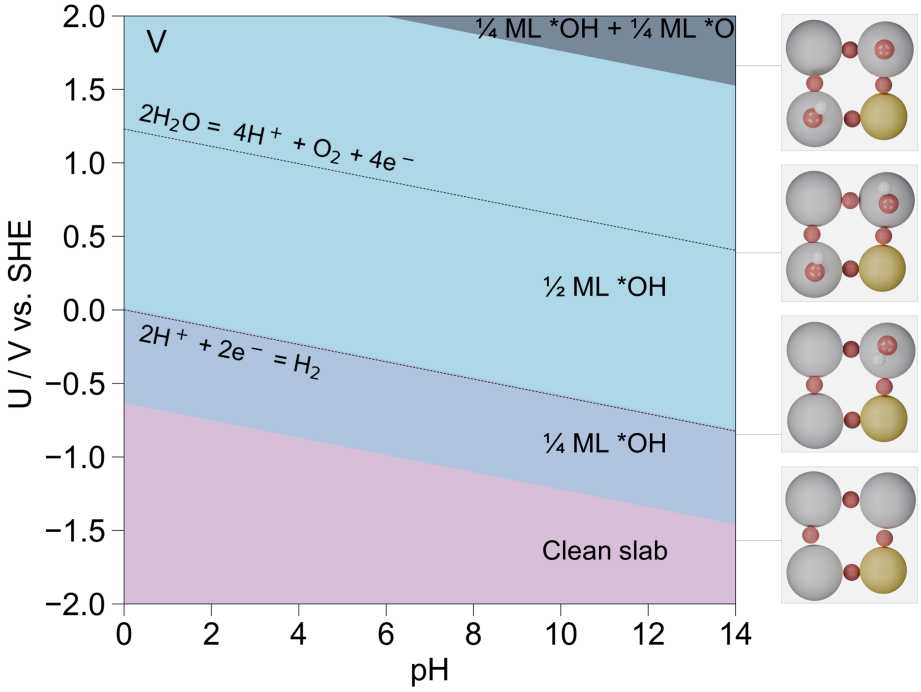

Figure S3. Surface Pourbaix diagram of V-doped Ta_2O_5(100)

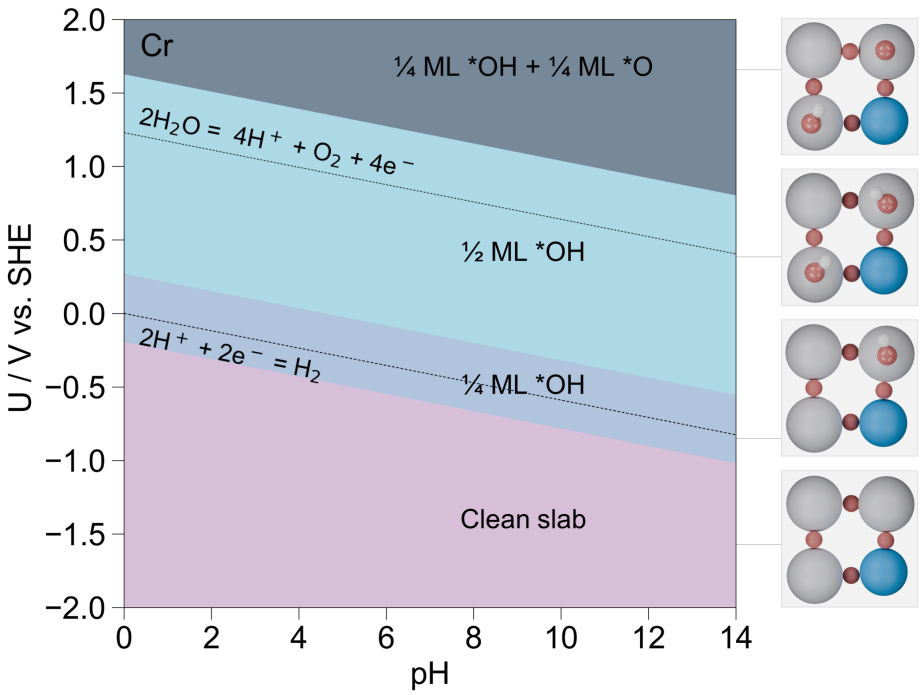

Figure S4. Surface Pourbaix diagram of Cr-doped Ta_2O_5(100)

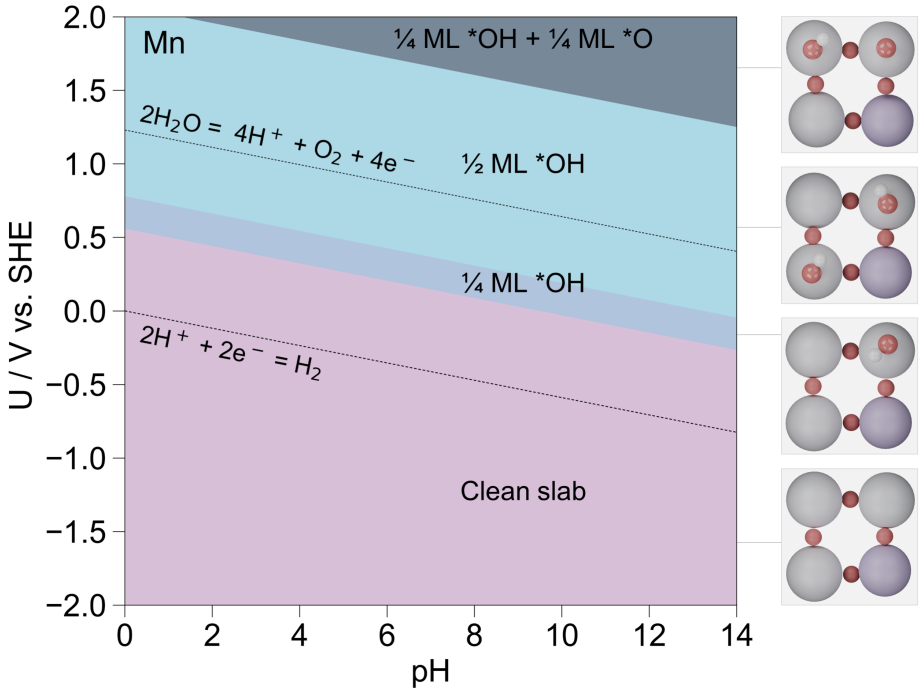

Figure S5. Surface Pourbaix diagram of Mn-doped Ta_2O_5(100)

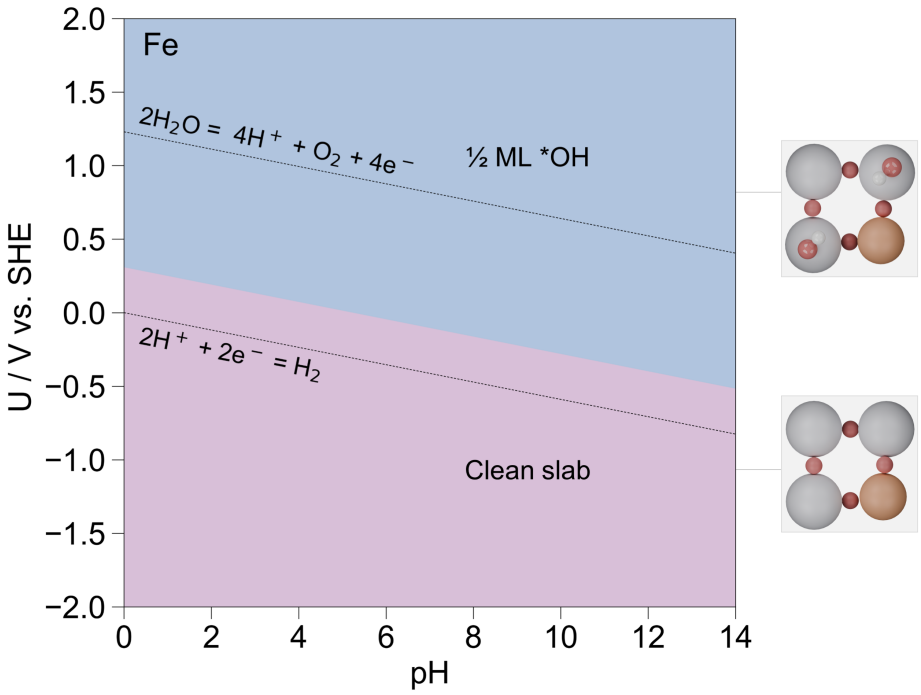

Figure S6. Surface Pourbaix diagra of Fe-doped Ta_2O_5(100)

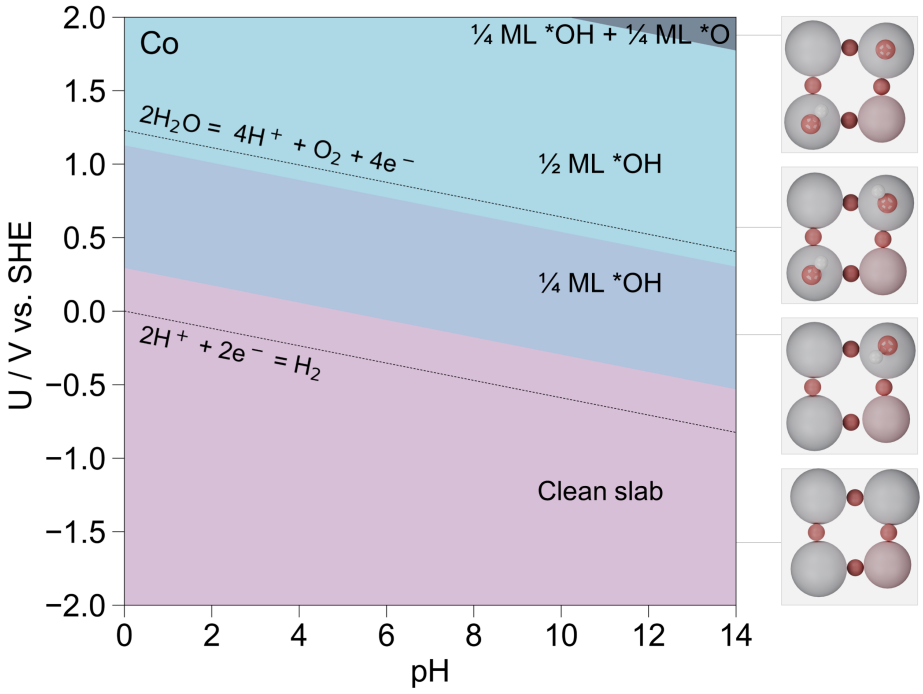

Figure S7. Surface Pourbaix diagram of Co-doped Ta_2O_5(100)

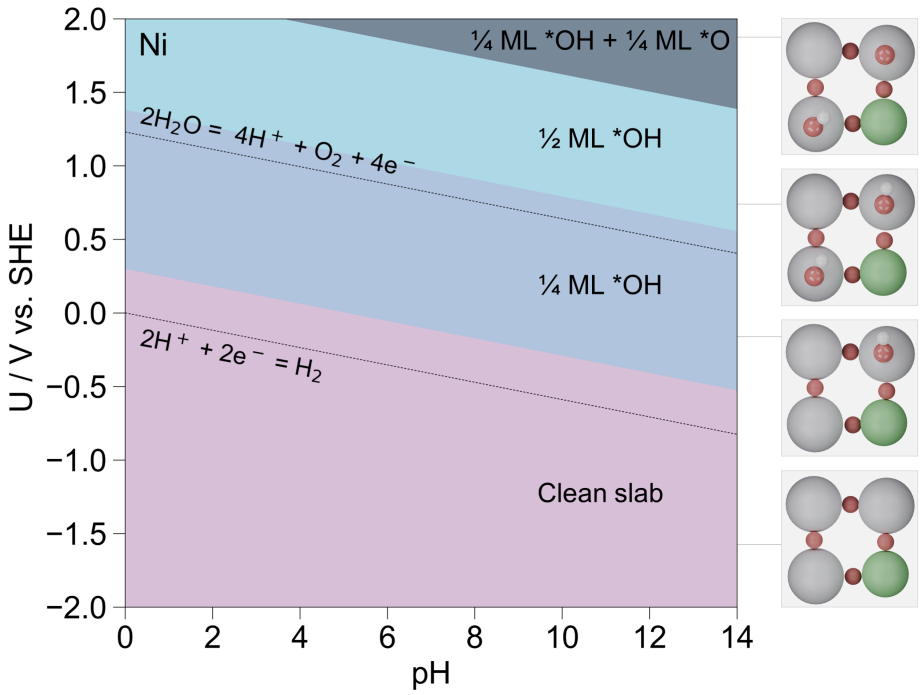

Figure S8. Surface Pourbaix diagram of Ni-doped Ta_2O_5(100)

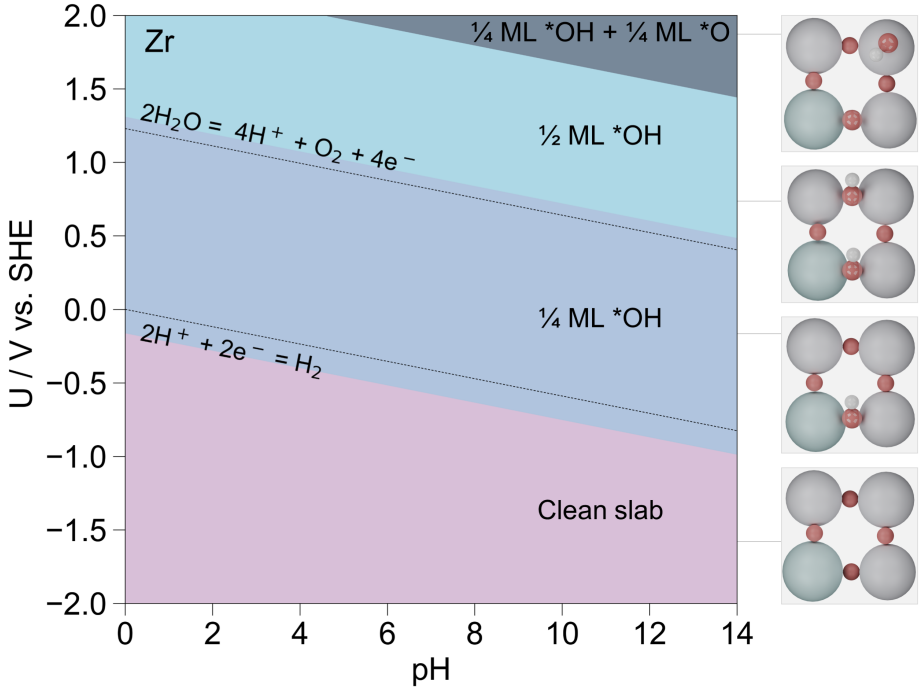

Figure S9. Surface Pourbaix diagram of Zr-doped Ta_2O_5(100)

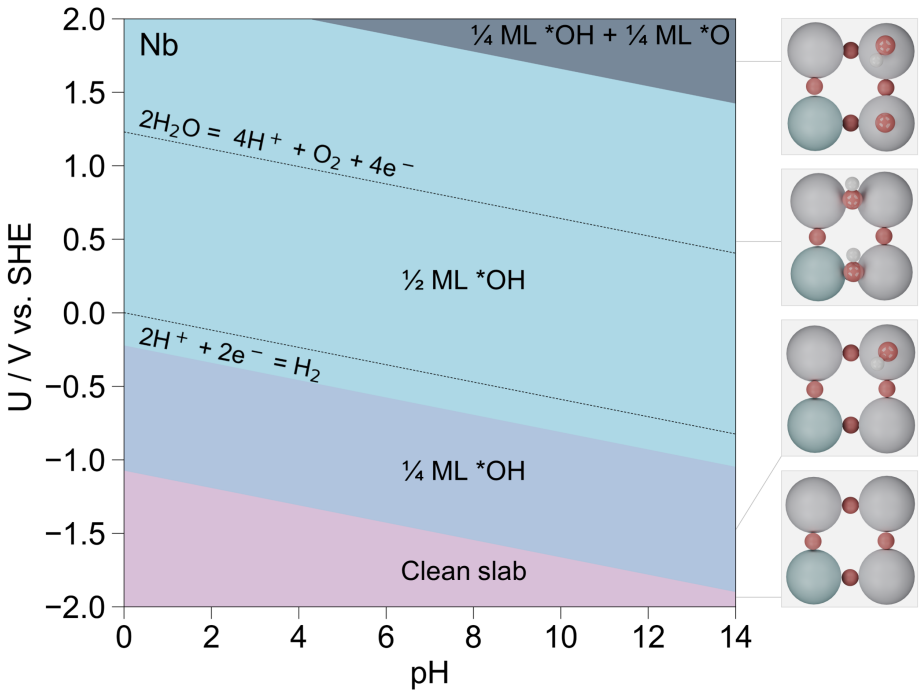

Figure S10. Surface Pourbaix diagram of Nb-doped Ta_2O_5(100)

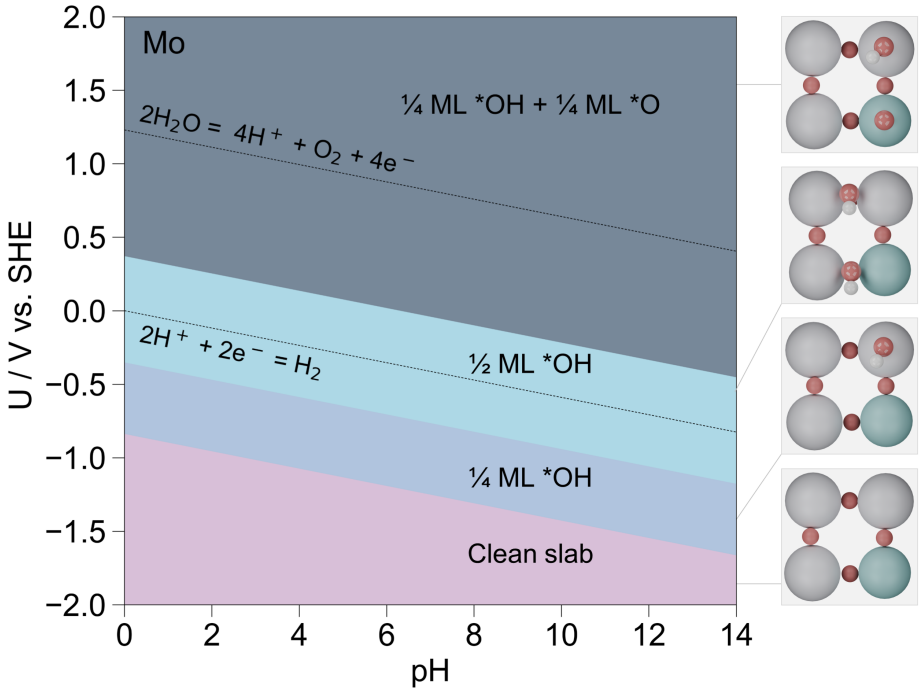

Figure S11. Surface Pourbaix diagram of Mo-doped Ta_2O_5(100)

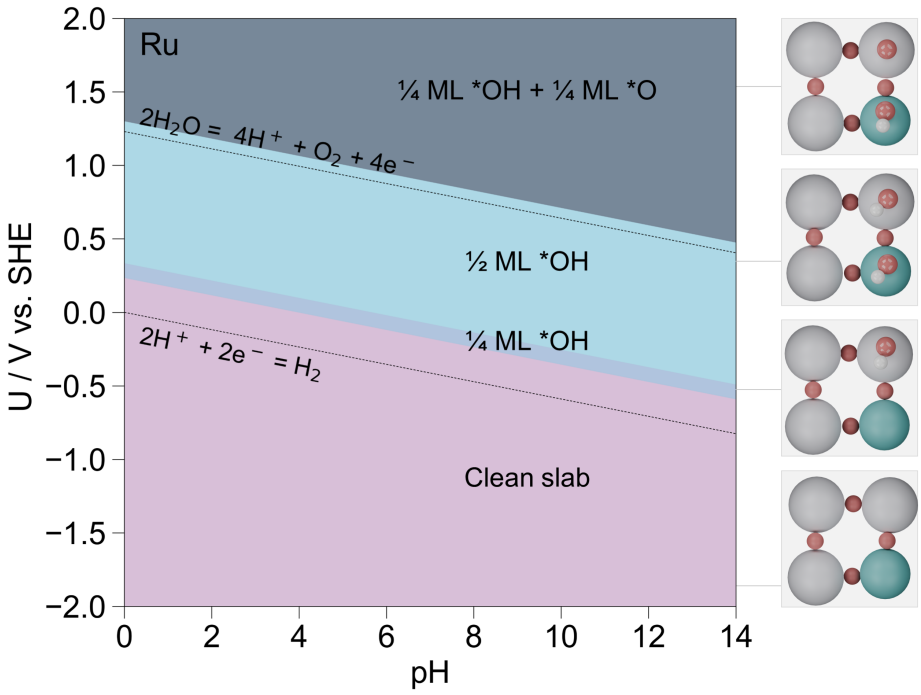

Figure S12. Surface Pourbaix diagram of Ru-doped Ta_2O_5(100)

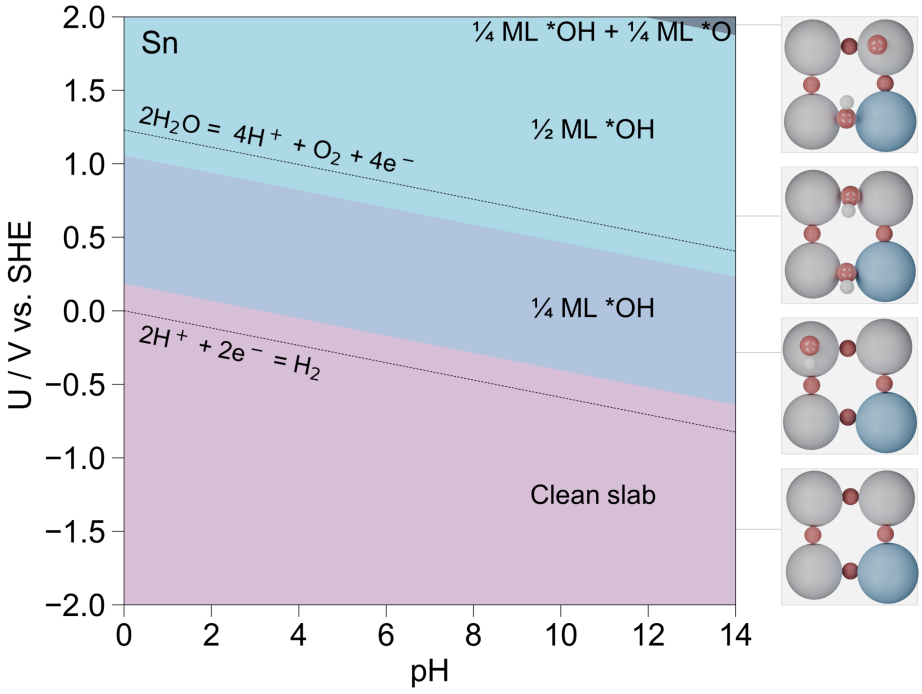

Figure S13. Surface Pourbaix diagram of Sn-doped Ta_2O_5(100)

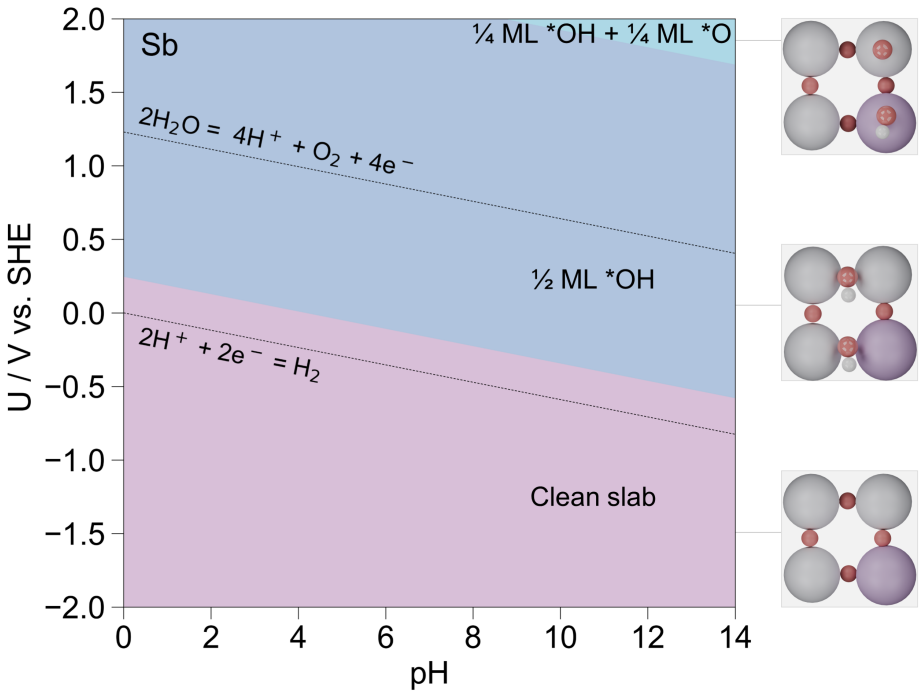

Figure S14. Surface Pourbaix diagram of Sb-doped Ta_2O_5(100)

References

1. J. Rossmeisl, A. Logadottir and J. K. Nørskov, *Chem. Phys.*, 2005, **319**, 178-184.
2. J. Rossmeisl, Z. W. Qu, H. Zhu, G. J. Kroes and J. K. Nørskov, *J. Electroanal. Chem.*, 2007, **607**, 83-89.
3. M. Bajdich, M. García-Mota, A. Vojvodic, J. K. Nørskov and A. T. Bell, *J. Am. Chem. Soc.*, 2013, **135**, 13521-13530.
4. J. K. Nørskov, J. Rossmeisl, A. Logadottir, L. Lindqvist, J. R. Kitchin, T. Bligaard and H. Jónsson, *J. Phys. Chem. B*, 2004, **108**, 17886-17892.
5. M. López, K. S. Exner, F. Viñes and F. Illas, *Adv. Theory Simul.*, 2023, **6**, 2200217.